Supplement of Atmos. Chem. Phys., 17, 5007–5033, 2017
http://www.atmos-chem-phys.net/17/5007/2017/
doi:10.5194/acp-17-5007-2017-supplement

Atmospheric Chemistry and Physics Open Access EGU

Supplement of

Validation of OMI, GOME-2A and GOME-2B tropospheric NO_2, SO_2 and HCHO products using MAX-DOAS observations from 2011 to 2014 in Wuxi, China: investigation of the effects of priori profiles and aerosols on the satellite products

Yang Wang et al.

Correspondence to: Yang Wang (y.wang@mpic.de), Ang Li (angli@aiofm.ac.cn) and Cheng Liu (chliu81@ustc.edu.cn)

1 Effects of variations of the coincidence criteria on the validation

Because of the large ground pixel size of the satellite observations, MAX-DOAS results are averaged over a time period around the satellite overpass time to (partly) compensate the effect of horizontal gradients of the TG concentrations. In principle the time period is a function of the satellite pixel size, the wind speed and the life time of the trace gases. Although some factors change frequently, here we use one fixed time period for the long-term comparisons for simplicity. In this section, we test the effect on the satellite validation for four time periods including 1 hour, 2 hours, 3 hours and 4 hours around the satellite overpass time. Scatter plots of the average MAX-DOAS data over three time periods (1 hour, 3 hours and 4 hours) against those over 2 hours are shown in Fig. S1. The correlation coefficients are close to unity for all time periods. However, the slopes become systematically smaller for larger time periods (up to -10%) because of temporal smoothing. The results of the linear regressions and mean relative differences from the comparisons are also shown in Fig. S5a and will be discussed below together with the effect of the selected coincidence area of the satellite products.

In principle for the satellite validation the satellite pixel closest to the MAX-DOAS instrument need to be selected. However, in order to minimise the random noise of the satellite data, it is useful to calculate the average of several satellite observations close to the measurement site (see e.g. Irie et al., 2012 and Ma et al., 2013). As selection criterion, a distance between the centre of the satellite pixel and the measurement site can be specified. This optimum distance depends on many factors, such as the satellite ground pixel size, the selected time period over which the MAX-DOAS results are averaged, the expected horizontal gradients of the trace gas and uncertainties of the satellite data. A distance of < 20 km has been used for NO_2 comparisons (e.g. Ma et al., 2013 and Chan et al., 2015), 100 km for HCHO (De Smedt et al., 2015) and SO_2 (Theys et al., 2015). Irie et al. (2012) already found that the correlations and slopes of the linear regressions of the NO_2 tropospheric VCDs from OMI and GOME-2A against those from MAX-DOAS observations depend systematically on the distance to the MAX-DOAS station.

We test the effect of the variation of the distance between 10 km to 75 km on the comparison between the satellite data (OMI and GOME-2) and the MAX-DOAS data for all three TGs. The areas for the four radii (10km, 20km, 50km and 75km) and the pixel sizes of OMI and GOME-2 are shown in the earth view image downloaded from the Google Earth service in Fig. S2a. For distances larger than 20 km, the cities of Suzhou, Changzhou, Huzhou and Nantong are included in the area. Because of transport of the pollutants between the cities and the different residence times, different horizontal distributions of the NO_2, SO_2 and HCHO VCDs are found around Wuxi as shown in Figs. S2b, c and d, respectively. HCHO has a smoother distribution than SO_2, which is smoother than NO_2. The satellite data for pixels with the distances of 0-10km, 10-20km, 20-50km and 50-75km to the MAX-DOAS station are compared with the MAX-DOAS results.

We compare both the results for individual satellite pixels and daily averages for the four radii with the average MAX-DOAS data over 2 hours around the satellite overpass time. The comparisons for OMI NO_2, SO_2 and HCHO for pixels with distances of 0-10km, 10-20km, 20-50km and 50-75km are shown in Fig. S3a, b and c, respectively (the comparisons for pixels with the distances of <10km, <20km, <50km and <75km are shown in Fig. S4). We use the SO_2 OMI product from BIRA for this study, because it shows in general a higher correlation with the MAX-DOAS data. We found that the linear regressions for the daily averaged data are quite similar to those for the individual pixel data. Only the correlation coefficients are higher. The results of the linear regressions and the mean relative differences for the two distance categories as indicated in Fig. S3 and S4 are shown in Fig. S5 b and c, respectively. The slopes decrease with increasing distance for the three gases. The decrease of the slopes (from 0.75 to 0.49 and R^2 from 0.66 to 0.29) are stronger for NO_2 than for SO_2 and HCHO. This finding is consistent with the typically stronger horizontal inhomogeneity of NO_2. The mean differences for HCHO show almost no dependence on the distance. This finding can be explained by the more homogenous distribution of HCHO compared to NO_2 and SO_2. A significant decrease of the slopes from 0.73 to 0.50 and the R^2 from 0.65 to 0.44 is found for NO_2 with increasing distance over 20km. A decrease of the slope is also found for SO_2 for the distances larger than 20km. From these findings we conclude that 20km is a reasonable distance to select OMI NO_2 and SO_2 data for conditions similar to those at Wuxi. In contrast, for HCHO we select a distance of 50 km. Although for such distances the slope is smaller than for shorter distances, we find nearly identical mean differences. Because of this finding and the rather high noise of the HCHO satellite data we select a distance of 50 km, for which the number of available measurements largely increases. The comparison of Fig. S5a and b indicates that the effect of time periods used for averaging the MAX-DOAS results on the validation study is much smaller than the effect of distances for selecting the satellite data. Thus we apply the time period of 2 hours around the satellite overpass time in this study.

Similar results for GOME-2 data as those for OMI shown in Fig. S5 are shown in Fig. S6. The O3M-SAF GOME-2A SO_2 product from DLR is used for this sensitivity study. Also for the GOME-2 SO_2 data set the effect of the horizontal coincidence criterion is larger than the effect of the time period for the averaging of the MAX-DOAS data is found. Thus also 2 hours around the satellite overpass time will be used for GOME-2 comparisons in this study. The largest changes of the slopes for the three trace gases are found around the distance of 10km, but the results for the selection criterion of 0-10km should be treated with care because of the low number of available measurements. The changes of the slopes for distances larger than 20km are smaller than 0.06 for NO_2 and 0.04 for HCHO, but are larger for SO_2. However, the results of the linear regressions for SO_2 should again be treated with care because of the rather low correlation coefficients. From these results we select 50km as a reasonable distance for GOME-2 data of NO_2, SO_2 and HCHO.

In summary, in the validation studies (section 3) of the main manuscript, the MAX-DOAS results are selected within the period from 12:30 LT to 14:30 LT for the comparisons with OMI and from 08:30 LT to 10:30 LT for the comparisons with GOME-2A/B. The OMI NO_2 and SO_2 (HCHO) data are selected for satellite pixels with the distance of <20km (<50km) from the Wuxi station. The GOME-2A/B data of the three species are selected for the distances < 50km.

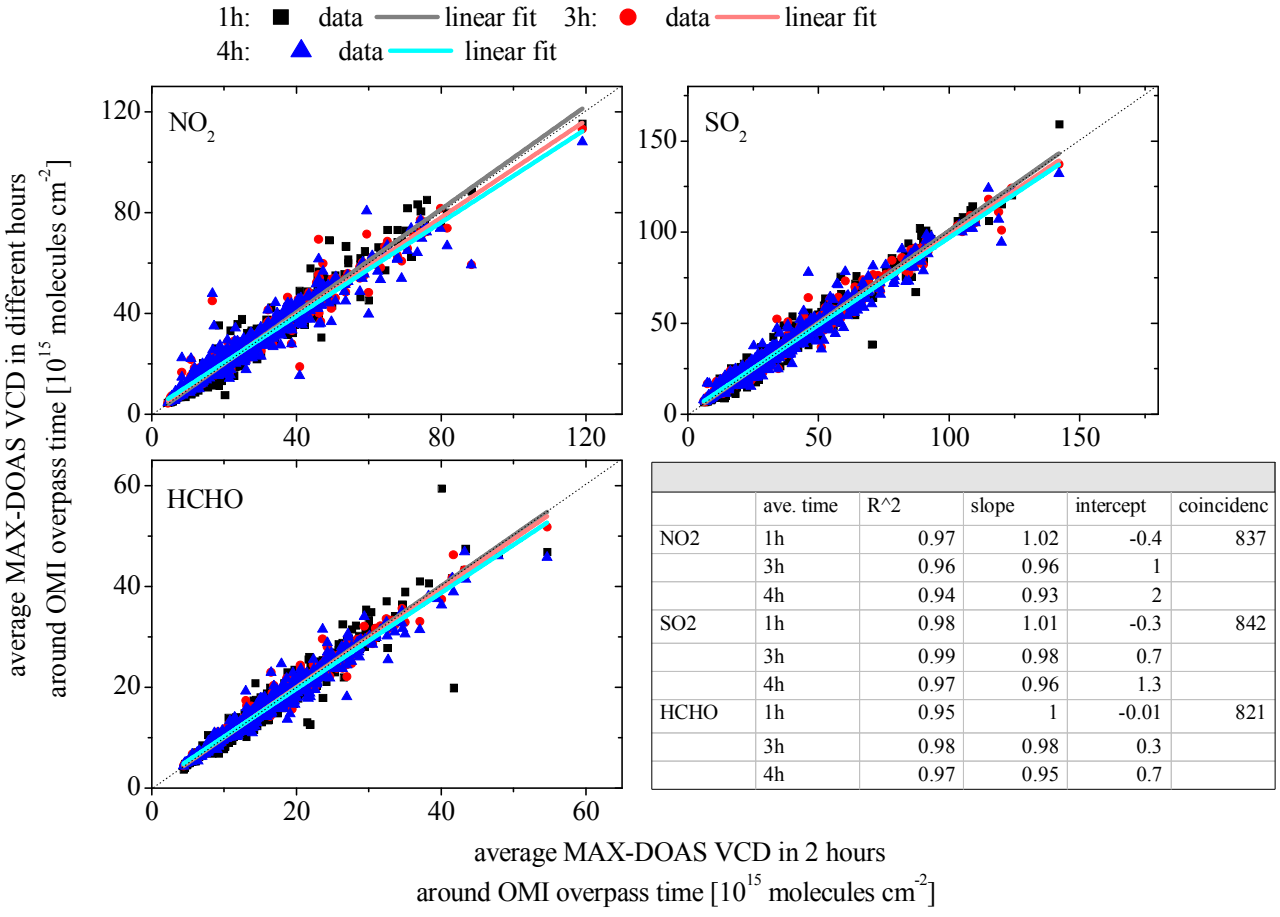

	ave. time	R^2	slope	intercept	coincidenc
NO2	1h	0.97	1.02	-0.4	837
	3h	0.96	0.96	1	
	4h	0.94	0.93	2	
SO2	1h	0.98	1.01	-0.3	842
	3h	0.99	0.98	0.7	
	4h	0.97	0.96	1.3	
HCHO	1h	0.95	1	-0.01	821
	3h	0.98	0.98	0.3	
	4h	0.97	0.95	0.7	

Figure S1: Averaged NO_2 (a), SO_2 (b) and HCHO (c) tropospheric VCDs derived from MAX-DOAS observations in time periods of 1 hour (black dots), 3 hours (red dots) and 4 hours (blue dots) around the OMI overpass time plotted against those in the time period of 2 hours around the OMI overpass time. The linear regression lines for each time period and each species are plotted in each subfigure. The corresponding parameters are listed in the table.

(a)

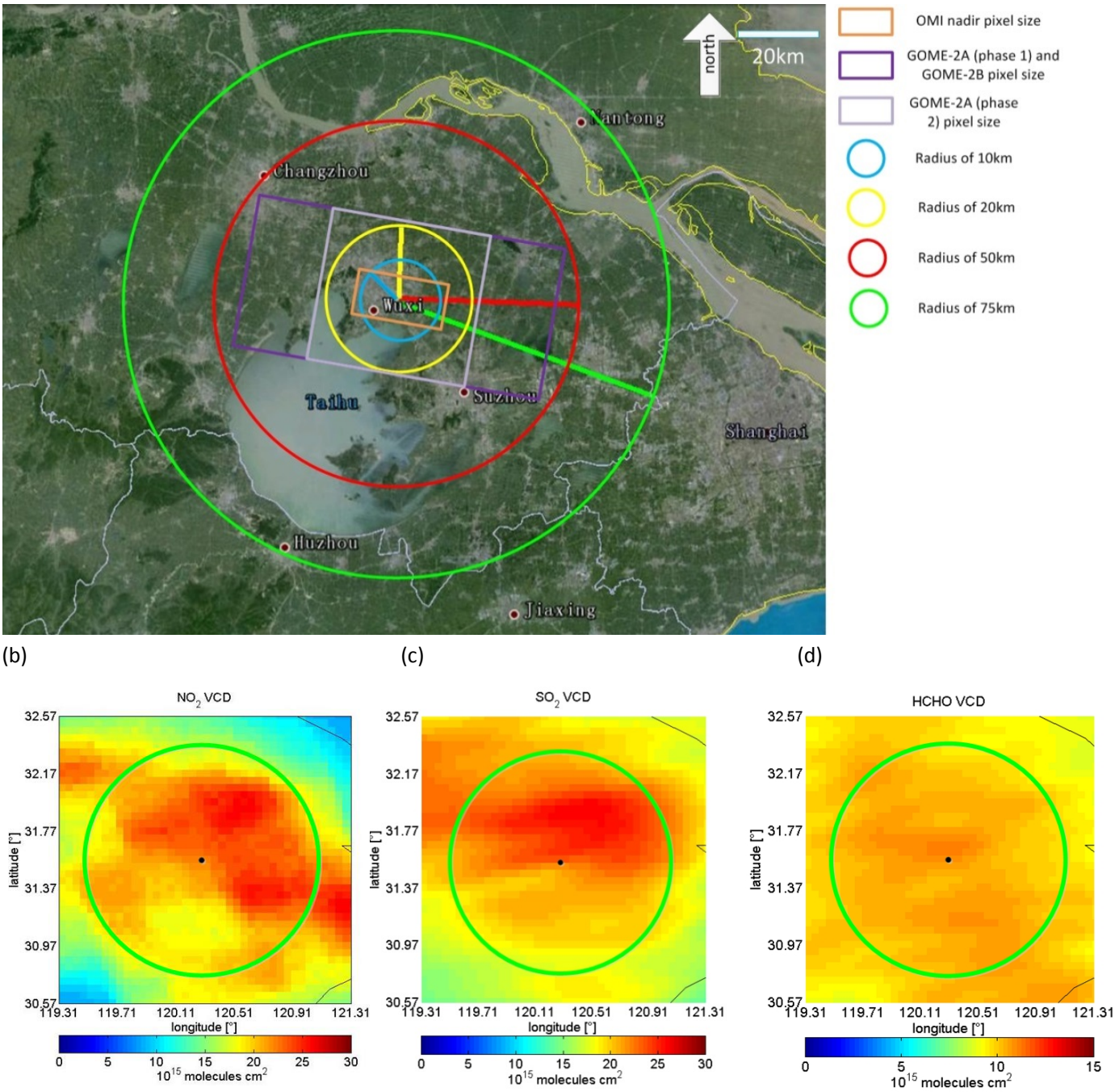

Figure S2: Subfigure (a) shows the earth image around Wuxi MAX-DOAS station from google earth service; the rectangles indicate the ground pixel sizes of the different satellite instruments used in this study. (GOME2-A phase 1 and phase 2 corresponding to the periods before and after 15 July 2013); the circles indicate areas with different radii around Wuxi. The subfigures of (b), (c) and (d) show averaged VCDs of NO_2, SO_2 and HCHO for the same area as shown in (b-1); the black dots indicate the location of Wuxi and the green circles have a radius of 75km.

(a)

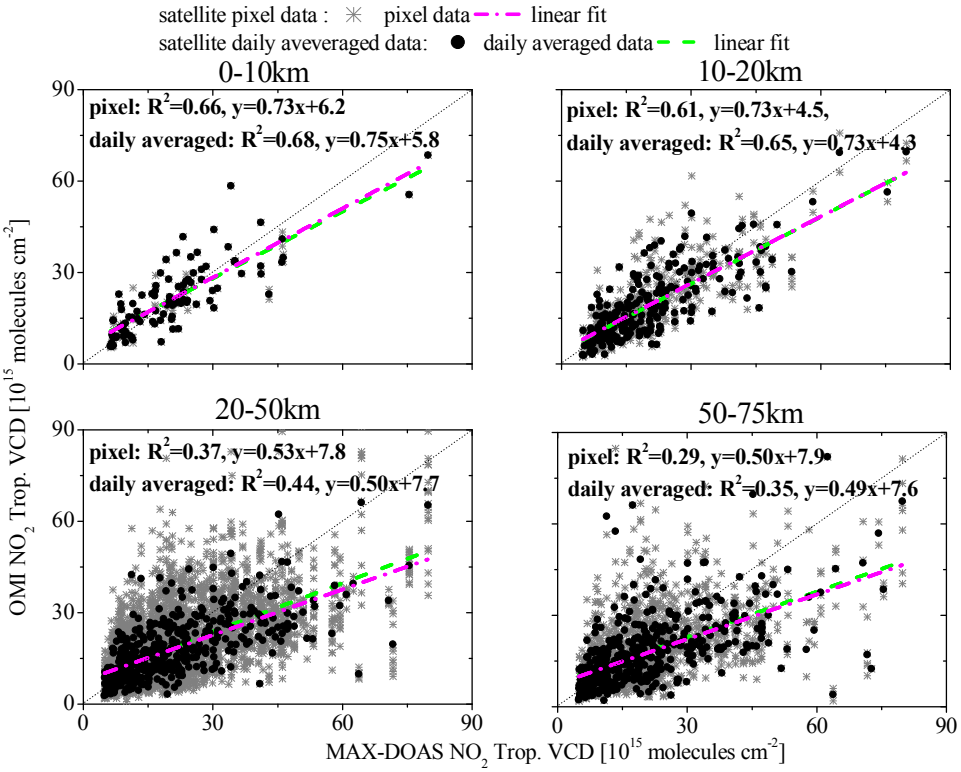
satellite pixel data : pixel data linear fit
satellite daily aveveraged data: daily averaged data linear fit
0-10km
pixel: R2=0.66, y=0.73x+6.2
daily averaged: R2=0.68, y=0.75x+5.8
10-20km
pixel: R2=0.61, y=0.73x+4.5,
daily averaged: R2=0.65, y=0.73x+4.3
20-50km
pixel: R2=0.37, y=0.53x+7.8
daily averaged: R2=0.44, y=0.50x+7.7
50-75km
pixel: R2=0.29, y=0.50x+7.9
daily averaged: R2=0.35, y=0.49x+7.6
OMI NO2 Trop. VCD [10^15 molecules cm^-2]
MAX-DOAS NO2 Trop. VCD [10^15 molecules cm^-2]

(b)

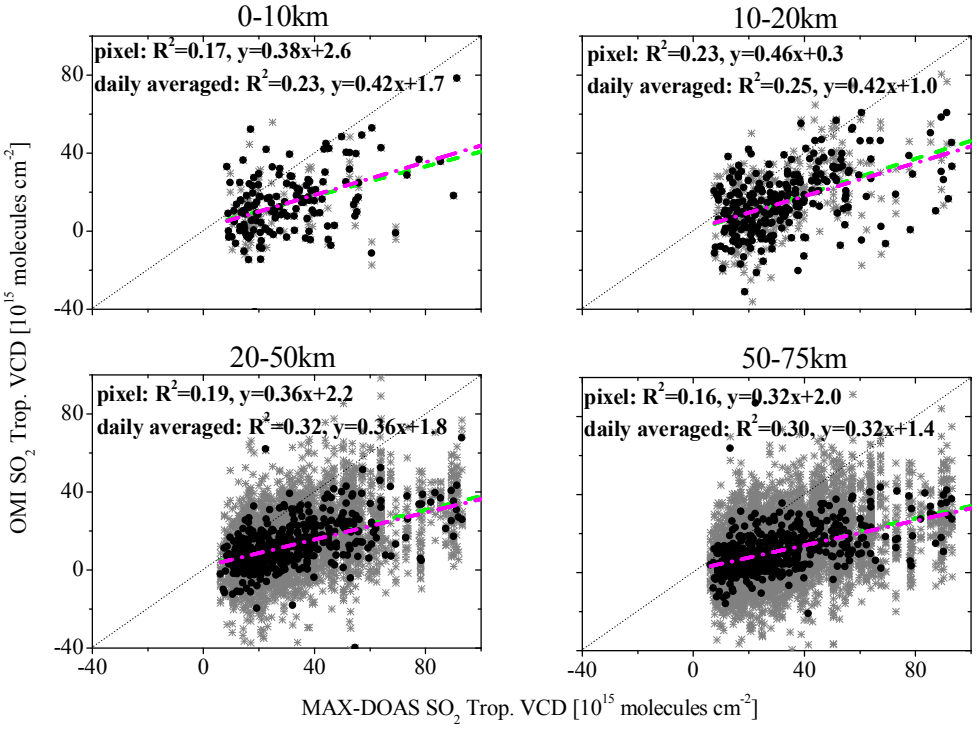
0-10km
pixel: R2=0.17, y=0.38x+2.6
daily averaged: R2=0.23, y=0.42x+1.7
10-20km
pixel: R2=0.23, y=0.46x+0.3
daily averaged: R2=0.25, y=0.42x+1.0
20-50km
pixel: R2=0.19, y=0.36x+2.2
daily averaged: R2=0.32, y=0.36x+1.8
50-75km
pixel: R2=0.16, y=0.32x+2.0
daily averaged: R2=0.30, y=0.32x+1.4
OMI SO2 Trop. VCD [10^15 molecules cm^-2]
MAX-DOAS SO2 Trop. VCD [10^15 molecules cm^-2]

(c)

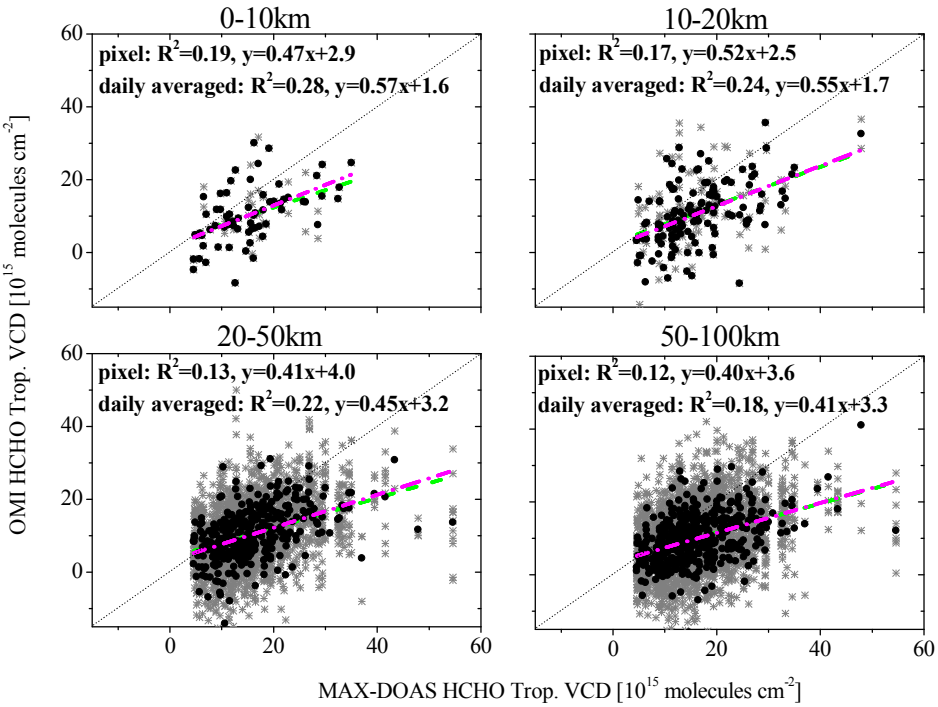

Figure S3: Tropospheric VCDs of NO_2 (a), SO_2 (b) and HCHO (c) derived from OMI observations for pixels within the distance bins of 0-10km, 10-20km, 20-50km and 50-75km away from the Wuxi MAX-DOAS station plotted against the coincident MAX-DOAS results. Only OMI data for the eCF<30% are included. For HCHO, only the data for a fit error < 7×10^{15} molecules cm^{-2} are included. The grey crosses and black dots show the data for individual satellite pixel and daily averaged data (averaged during two hours around the OMI overpass time), respectively. The linear regression lines and the parameters are shown in each subfigure for the pixel data (green dash lines) and daily averaged data (magenta dash-dot lines), respectively.

(a)

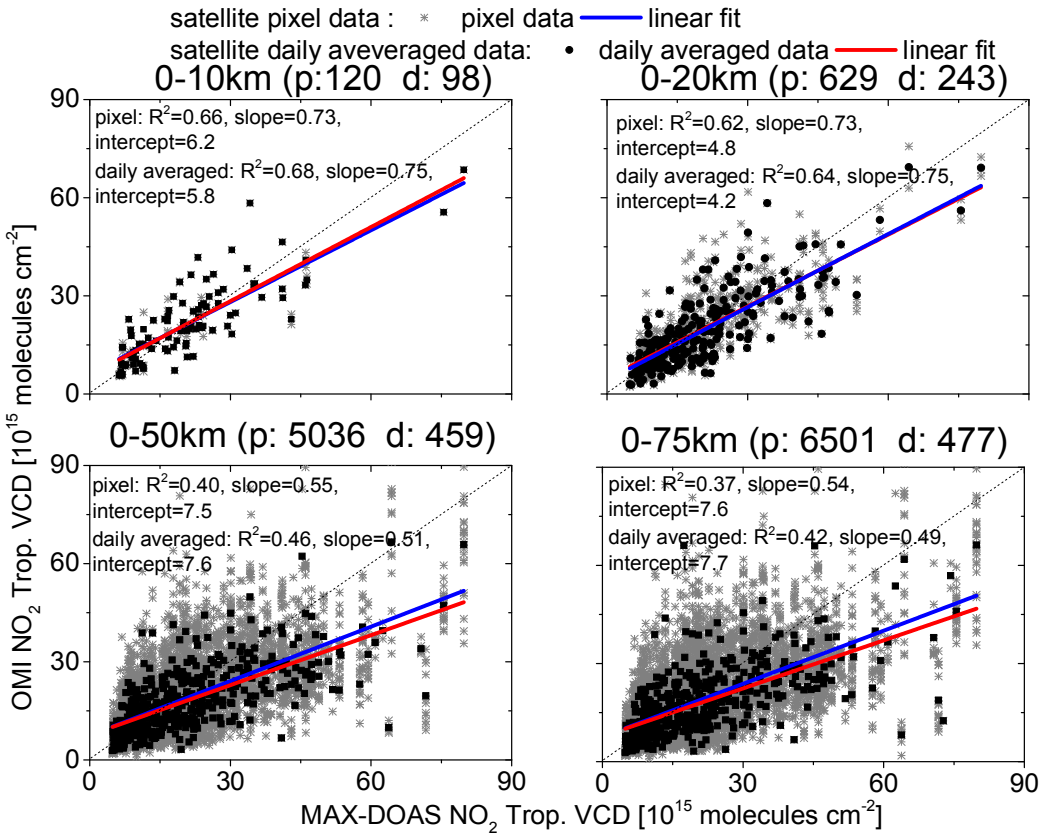
satellite pixel data : pixel data linear fit
satellite daily aveveraged data: daily averaged data linear fit
0-10km (p:120 d: 98)
pixel: R2=0.66, slope=0.73, intercept=6.2
daily averaged: R2=0.68, slope=0.75, intercept=5.8
0-20km (p: 629 d: 243)
pixel: R2=0.62, slope=0.73, intercept=4.8
daily averaged: R2=0.64, slope=0.75, intercept=4.2
0-50km (p: 5036 d: 459)
pixel: R2=0.40, slope=0.55, intercept=7.5
daily averaged: R2=0.46, slope=0.51, intercept=7.6
0-75km (p: 6501 d: 477)
pixel: R2=0.37, slope=0.54, intercept=7.6
daily averaged: R2=0.42, slope=0.49, intercept=7.7
OMI NO2 Trop. VCD [10^15 molecules cm^-2]
MAX-DOAS NO2 Trop. VCD [10^15 molecules cm^-2]

(b)

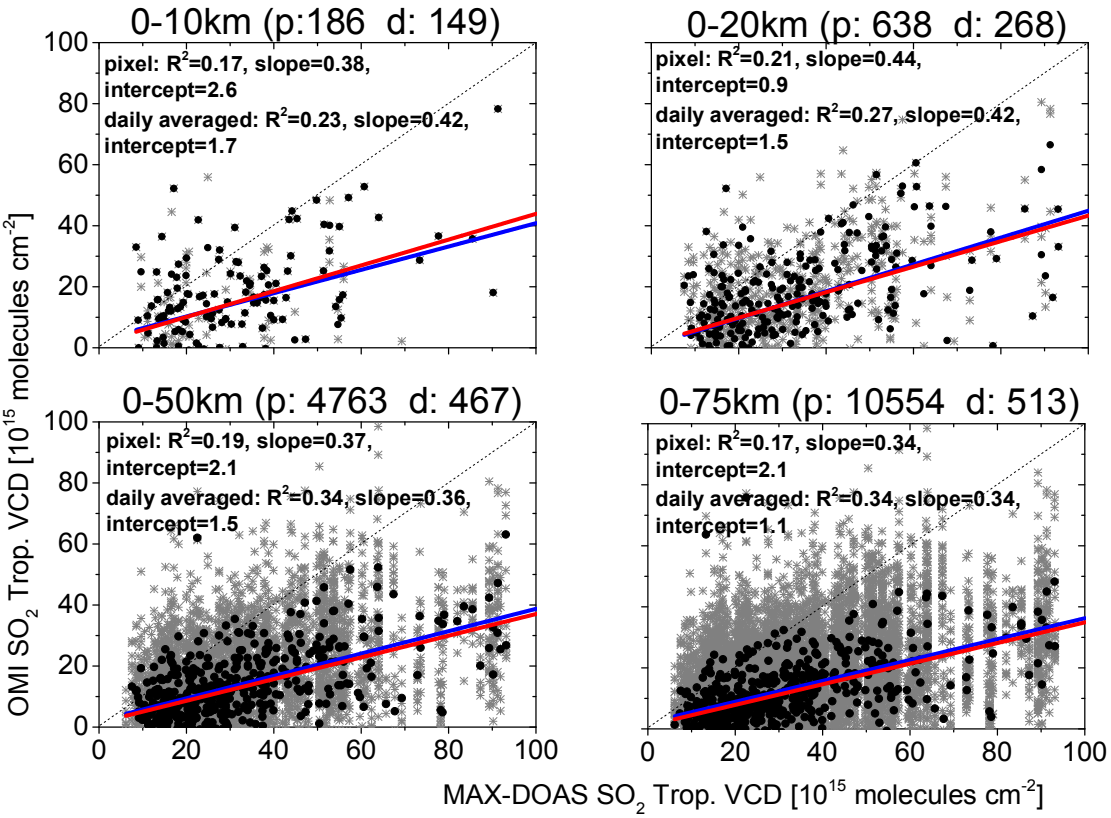
0-10km (p:186 d: 149)
pixel: R2=0.17, slope=0.38, intercept=2.6
daily averaged: R2=0.23, slope=0.42, intercept=1.7
0-20km (p: 638 d: 268)
pixel: R2=0.21, slope=0.44, intercept=0.9
daily averaged: R2=0.27, slope=0.42, intercept=1.5
0-50km (p: 4763 d: 467)
pixel: R2=0.19, slope=0.37, intercept=2.1
daily averaged: R2=0.34, slope=0.36, intercept=1.5
0-75km (p: 10554 d: 513)
pixel: R2=0.17, slope=0.34, intercept=2.1
daily averaged: R2=0.34, slope=0.34, intercept=1.1
OMI SO2 Trop. VCD [10^15 molecules cm^-2]
MAX-DOAS SO2 Trop. VCD [10^15 molecules cm^-2]

(c)

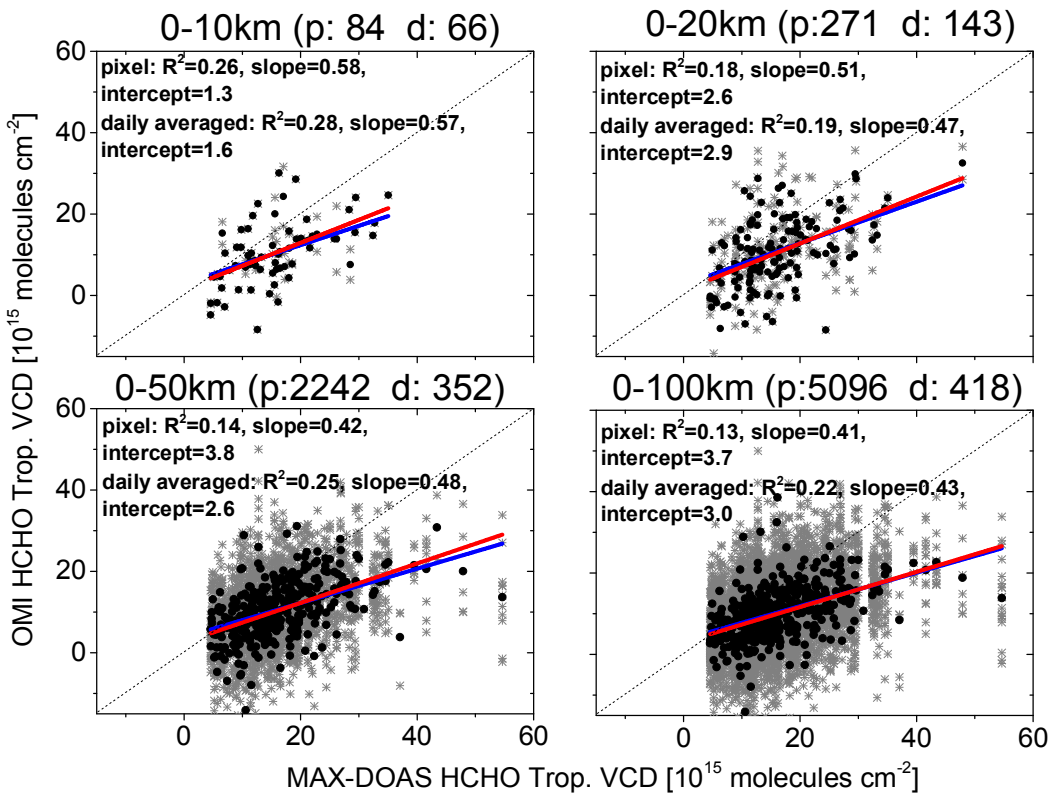

Figure S4: Tropospheric VCDs of NO_2 (a), SO_2 (b) and HCHO (c) derived from OMI observations for the pixel with the distance bins of 0-10km, 0-20km, 0-50km and 0-75km away from the Wuxi MAX-DOAS station are plotted against the coincident MAX-DOAS results. Only the OMI data for the eCF<30% are included. For HCHO, only the data for VCD fit error < 7×10^{15} molecules cm-2 are included. The grey and black dots show the data for each satellite pixel and daily averaged data (averaged during two hours around the OMI overpass time), respectively. The corresponding numbers of the pixels (p) and days (d) are shown in each subfigure. The linear regression lines and the parameters are shown in each subfigure for the pixel data (blue lines) and daily averaged data (red lines), respectively.

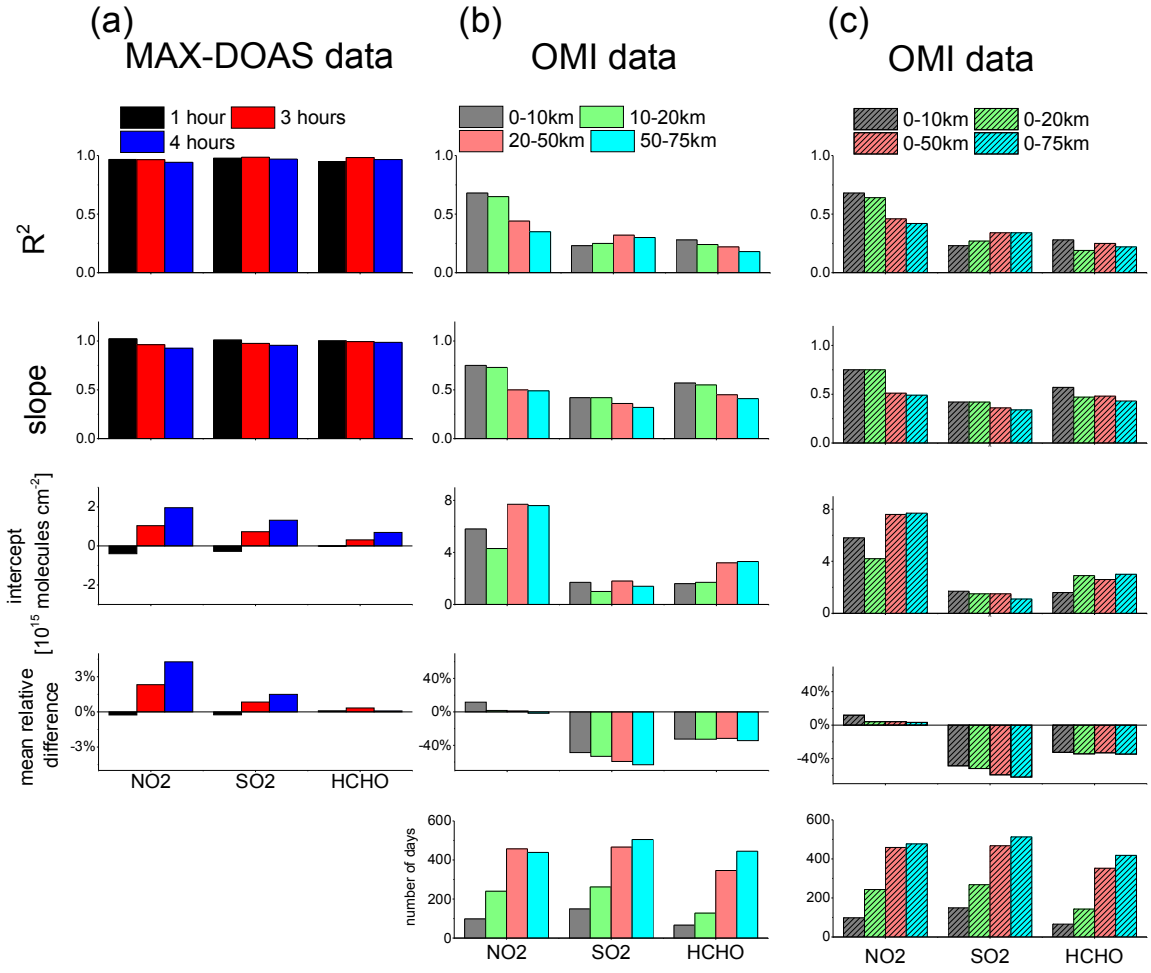

Figure S5: (a) R^2, slope and intercept of the linear regressions as well as the mean relative differences of the averaged MAX-DOAS tropospheric VCDs of NO_2, SO_2 and HCHO in the time periods of 1 hour, 3 hours and 4 hours around the OMI overpass time compared to those in the time period of 2 hours. (b) R^2, slope and intercept of the linear regressions as well as the mean relative differences of the averaged OMI tropospheric VCDs of NO_2, SO_2 and HCHO for the pixels within the distance bins of 0-10km, 10-20km, 20-50km and 50-75km compared to the coincident MAX-DOAS results. At the bottom also the numbers of the days for each comparison are shown. (c) Similar with (b), but for distance bins of 0-10km, 0-20km, 0-50km and 0-75km.

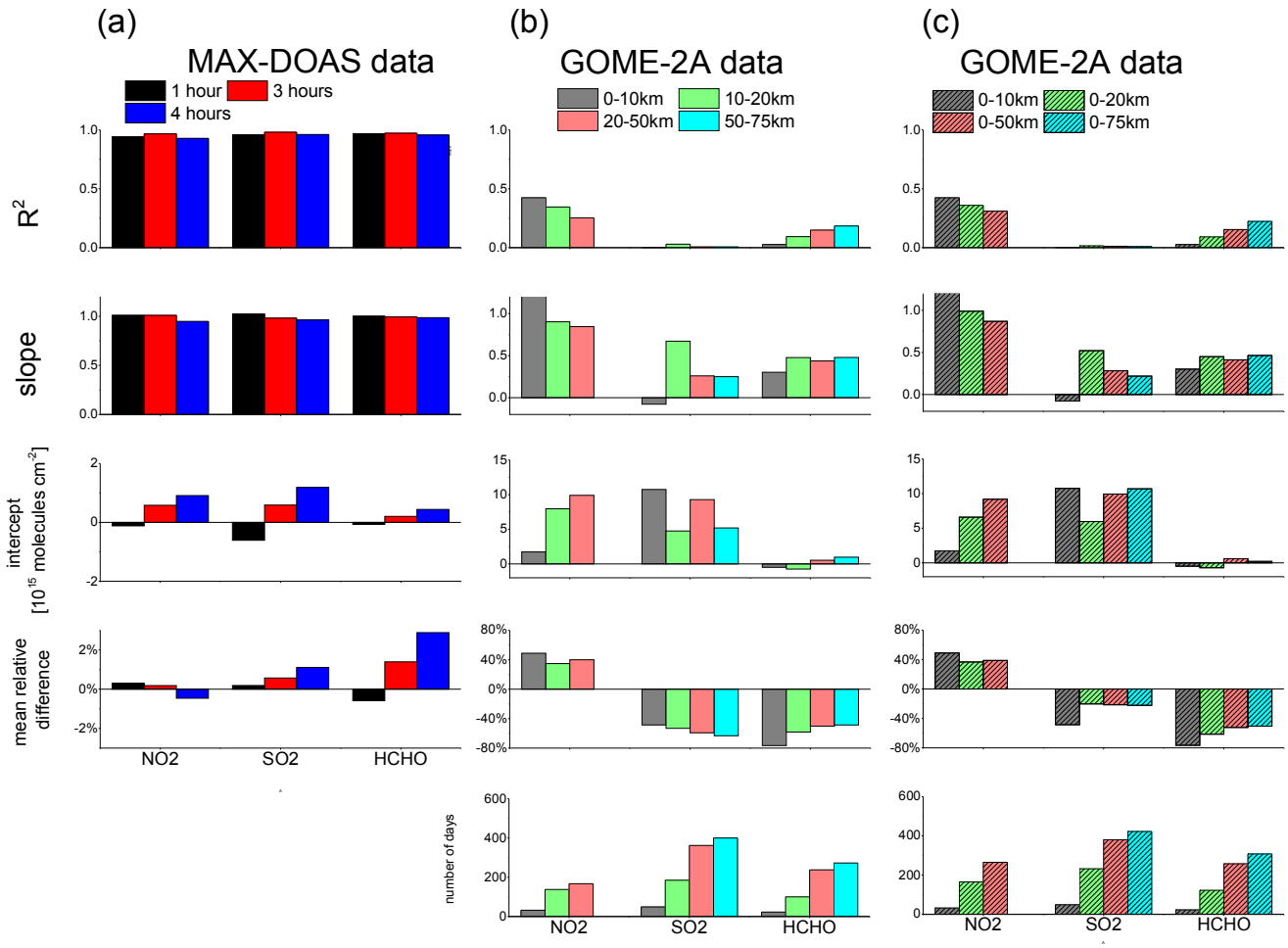

Figure S6: same as Fig. S5, but for GOME-2A data.

2 Cloud effect on MAX-DOAS tropospheric VCDs around the satellite overpass time

In the validation procedure the MAX-DOAS VCDs are averaged over a time period of ±one hour around the satellite overpass time. Typically about ten MAX-DOAS elevation sequences are recorded during that period, during which the cloud conditions can change. This effect is probably most important for the presence of broken cloud cover. Thus in order to evaluate the cloud effect on MAX-DOAS results, we compare the average MAX-DOAS VCDs derived from all measurements in ±1 hour around the satellite overpass time with those from the measurements under clear sky conditions only. Sky conditions are derived from MAX-DOAS measurements (Wang et al., 2015). The OMI overpass time of 13:30 local time (LT) is selected for the investigation of this effect, and similar features are expected for observations around the GOME-2 overpass time. Fig. S7a, b and c show scatter plots and linear regressions of the average MAX-DOAS VCDs from all the measurements in ±1 hour around the satellite overpass time against those under clear sky conditions for NO_2, SO_2 and HCHO, respectively. Almost 1:1 linear regression lines and correlation coefficients (R^2) (the Pearson's product moment correlation coefficient is applied in this paper) close to unity are found for all three species. To quantify the systematic differences of the TG VCDs, the corresponding mean differences (and standard deviations) are displayed in Fig. S7d for eCF<10% and eCF>10%, respectively. In general larger standard deviations are found for all three species for eCF>10%, indicating that larger deviations are related to larger eCF. Mean differences of 0.15×10^{15} molecules cm^{-2}, 0.02×10^{15} molecules cm^{-2} and 0.05×10^{15} molecules cm^{-2} (corresponding to 0.8%, 0.05% and 0.4% of the average VCDs) are found for NO_2, SO_2 and HCHO, respectively, indicating that the cloud effect on MAX-DOAS results is probably negligible for the satellite validations. Here it should be noted that the shown comparison results represent only situations, for which clear and cloudy conditions occur during the two-hour period around the satellite overpass time. Thus we cannot rule out that the errors for measurements under continuous cloud cover are larger. However

situations of continuous cloud cover are not relevant for this validation study, because for such conditions no meaningful satellite results can be obtained.

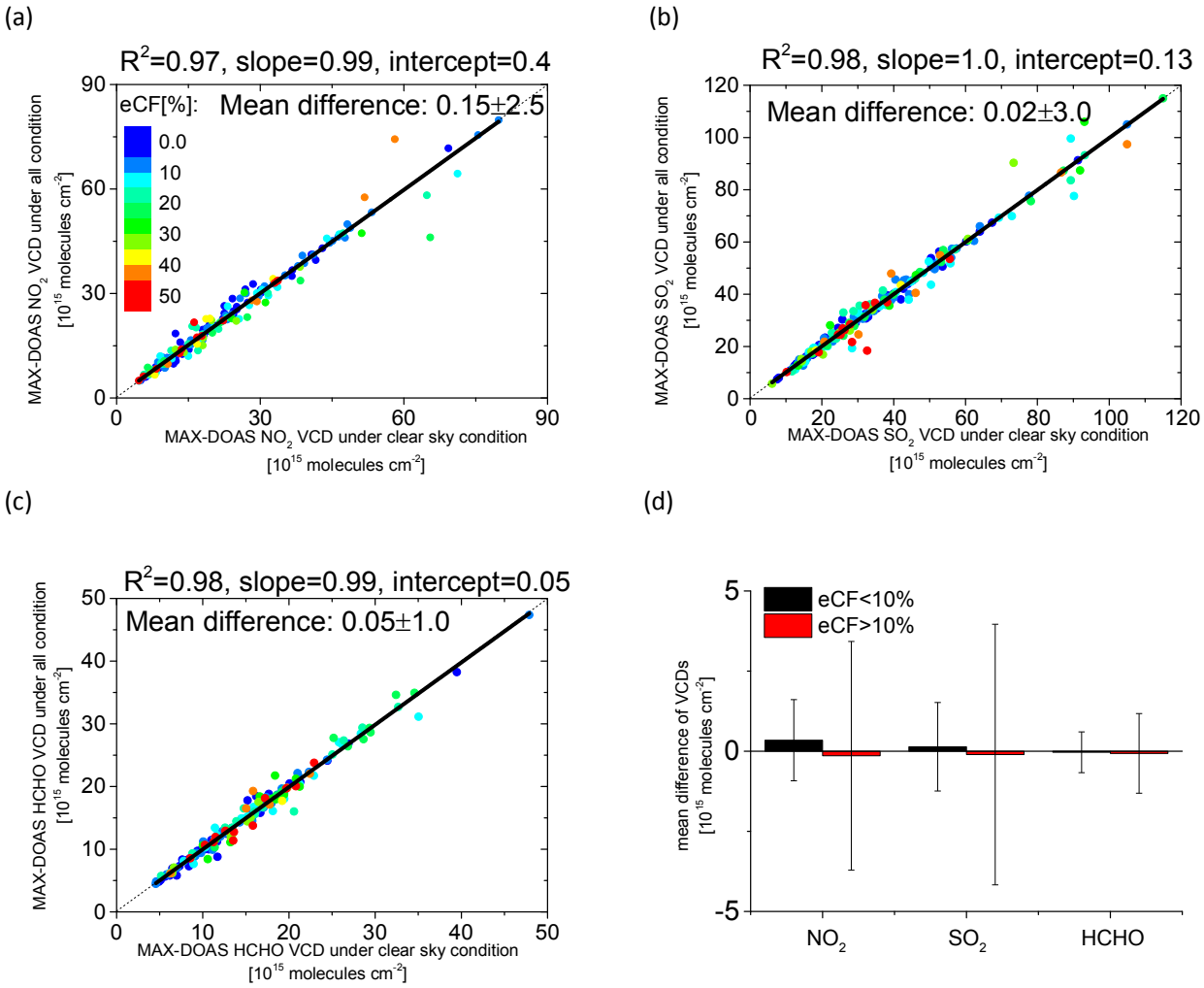

Figure S7: Daily averaged (during two hours around the OMI overpass time) NO_2 (a), SO_2 (b) and HCHO (c) tropospheric VCDs derived from MAX-DOAS observations under all sky conditions plotted against those under clear sky conditions. The colours indicate the eCF. The correlation coefficients, slopes, intercepts and mean differences ± standard deviation are displayed in each subfigure. The mean differences for eCF <10% and >10% are plotted in subfigure (d) with the error bars denoting the respective standard deviations.

3. Comparisons of AMFs for aerosols and low clouds

In this section we performed McArtim RTM simulations to estimate the effect of low level clouds on the TG AMFs compared to TG AMFs for aerosols. In the simulation the aerosol properties are assumed to be the same as in section 3.5 of the manuscript (two scenarios with either AOD of 0.8 or 1.5). The cloud properties are chosen to obtain the same radiance and O_4 SCDs (at 477nm) as for the aerosol scenarios, but the SSA is set to 1 and the asymmetry parameter g to 0.85. The simulations are performed for five satellite observation geometries as listed in Table 2 in the main manuscript. We chose two different cloud types: a) a homogeneous clouds with low optical depth covering the entire satellite pixel, and b) an optically thick cloud covering only 20% of the satellite pixel. It should be noted that the cloud extinction profiles can not unambiguously be determined based on the radiance and O_4 SCDs only. Thus we assumed two different types of clouds, which represent the most extreme cases: one case is a 'near-surface cloud' with a constant extinction starting from surface. For this cloud type the cloud top height is then derived based on O_4 SCDs; another cloud type is a 'lifted cloud' with the fixed vertical extension of 400 m (constant extinction in the cloud layer). For this cloud type the height of the cloud center is derived from the O_4 SCDs. Thus, in total all simulations are performed for four types of clouds, which are referred to as 'near-surface homogeneous clouds',

'near-surface partial clouds', 'lifted homogeneous clouds', and 'lifted partial clouds'. The comparisons of the corresponding sun-normalized radiances and O_4 SCDs between the aerosol profiles and with the derived cloud profiles are shown in Fig. S8 and S9, respectively. The derived cloud extinction profiles are shown in Fig. S10. Here it should be noted that the simulations for the near-surface homogeneous clouds can not match the O_4 SCD derived for the aerosols with AOD of 1.5. Finally the AMFs for the derived clouds are compared with those for the corresponding aerosols for the different observation geometries. The corresponding relative differences are shown in Fig. S11. In general the differences are smaller than 10% for NO_2, and 5% for SO_2 and HCHO, except for the g3 geometry, for which the NO_2 AMF difference amounts up to 20%. Thus we conclude that in general the influence of residual clouds on the satellite TG retrievals is of importance. Here it should be noted that especially over polluted regions situations with eCF<10% and CTP > 900 hPa typically represent cases with aerosol pollution. If in addition residual clouds are present, they typically co-exist with high aerosol amounts. Thus our simulation results (based on pure cloudy cases without aerosols) represent not typical but rather extreme cases.

(a)

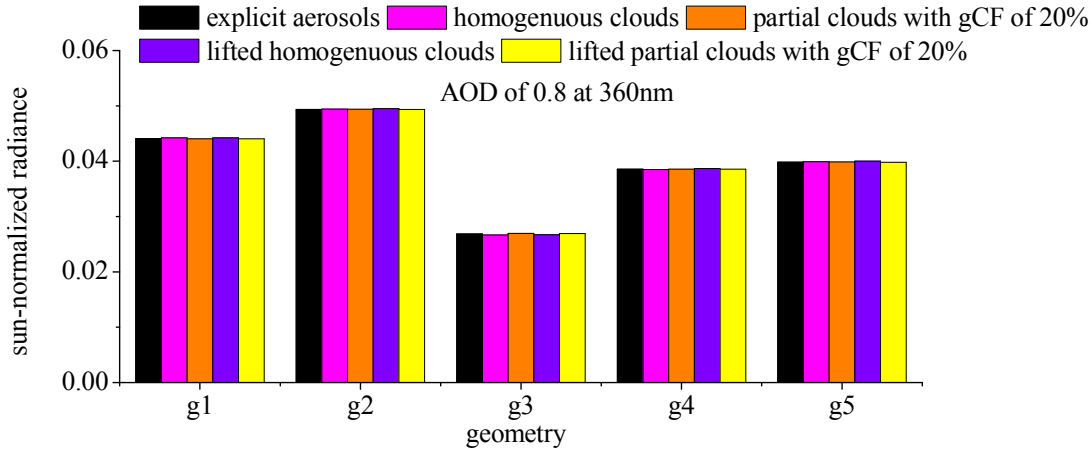

(b)

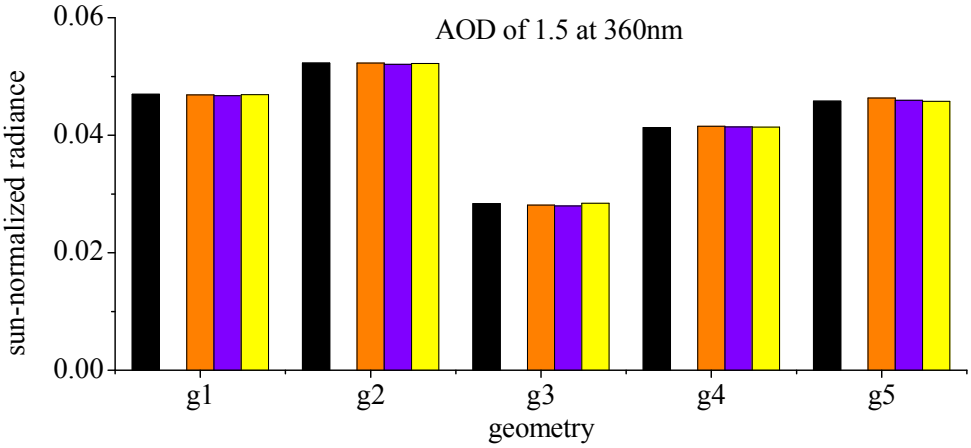

Figure S8: sun-normalized radiances simulated by RTM at 477nm for the two aerosol cases and the different clouds scenarios shown in Fig. S10. The different labels at the x-axis indicate different observation geometries (see Table 2 in the main text). The radiances for the AOD of 0.8 are shown in (a) and those for AOD of 1.5 in (b).

(a)

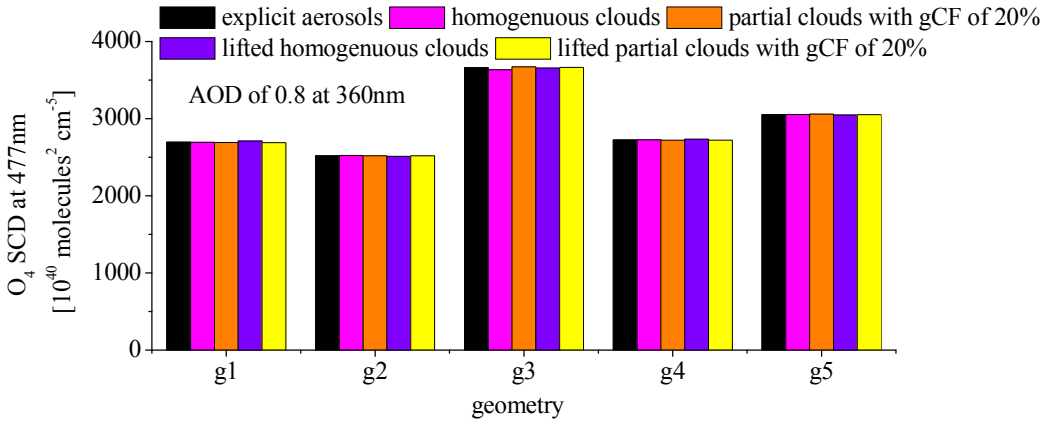

(b)

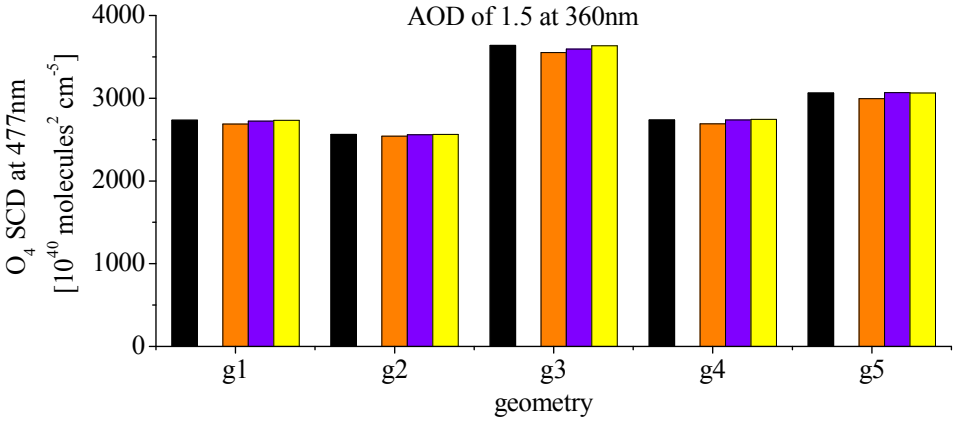

Figure S9: O_4 SCDs simulated by at 477nm for the two aerosol cases and the different clouds scenarios shown in Fig. S10.The different labels at the x-axis indicate different observation geometries (see Table 2 in the main text). The radiances for the AOD of 0.8 are shown in (a) and those for AOD of 1.5 in (b).

(a)

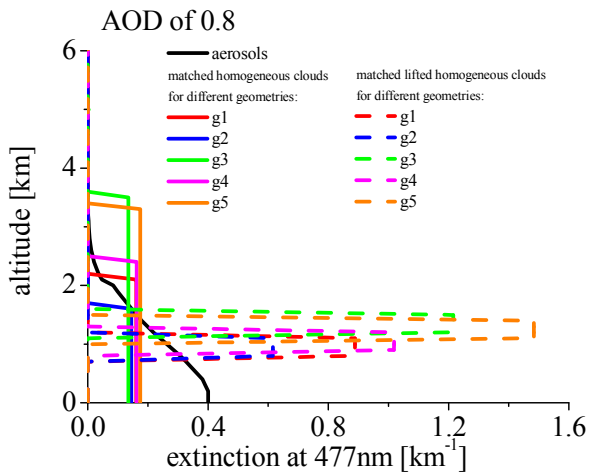

(b)

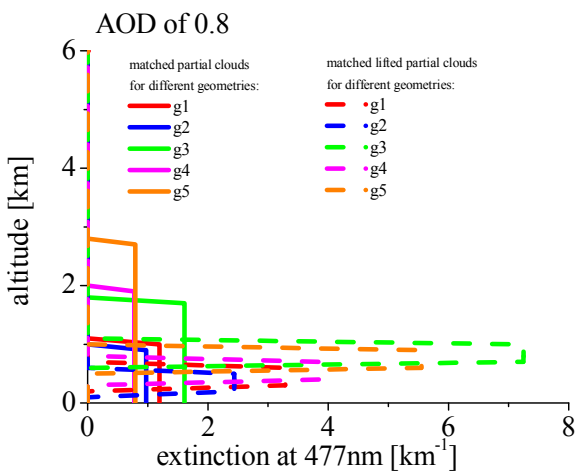

(c)

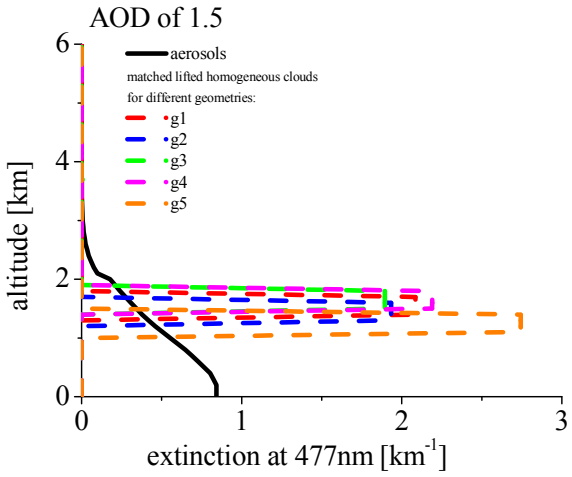

(d)

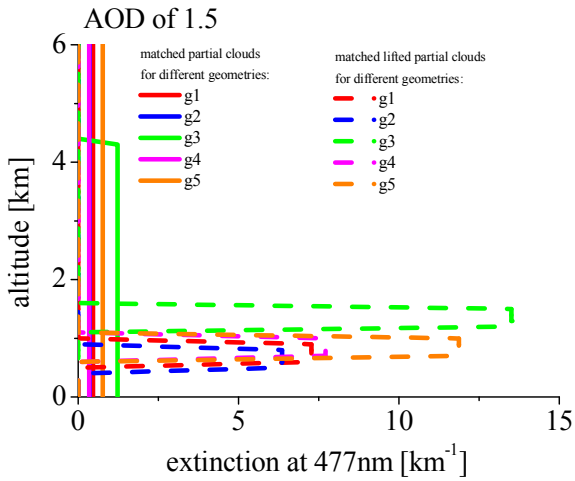

Figure S10: Derived cloud extinction profiles for the four cloud types and viewing geometries The black curves indicate the aerosol extinction profiles, the coloured lines the cloud extinction profiles. Homogeneous clouds and partial clouds (see text) are shown in (a) and (b). The solid and dashed curves indicate the near-surface and lifted clouds, respectively. (a) and (b) are for the aerosol of AOD of 0.8; (c) and (d) are for AOD of 1.5.

(a)

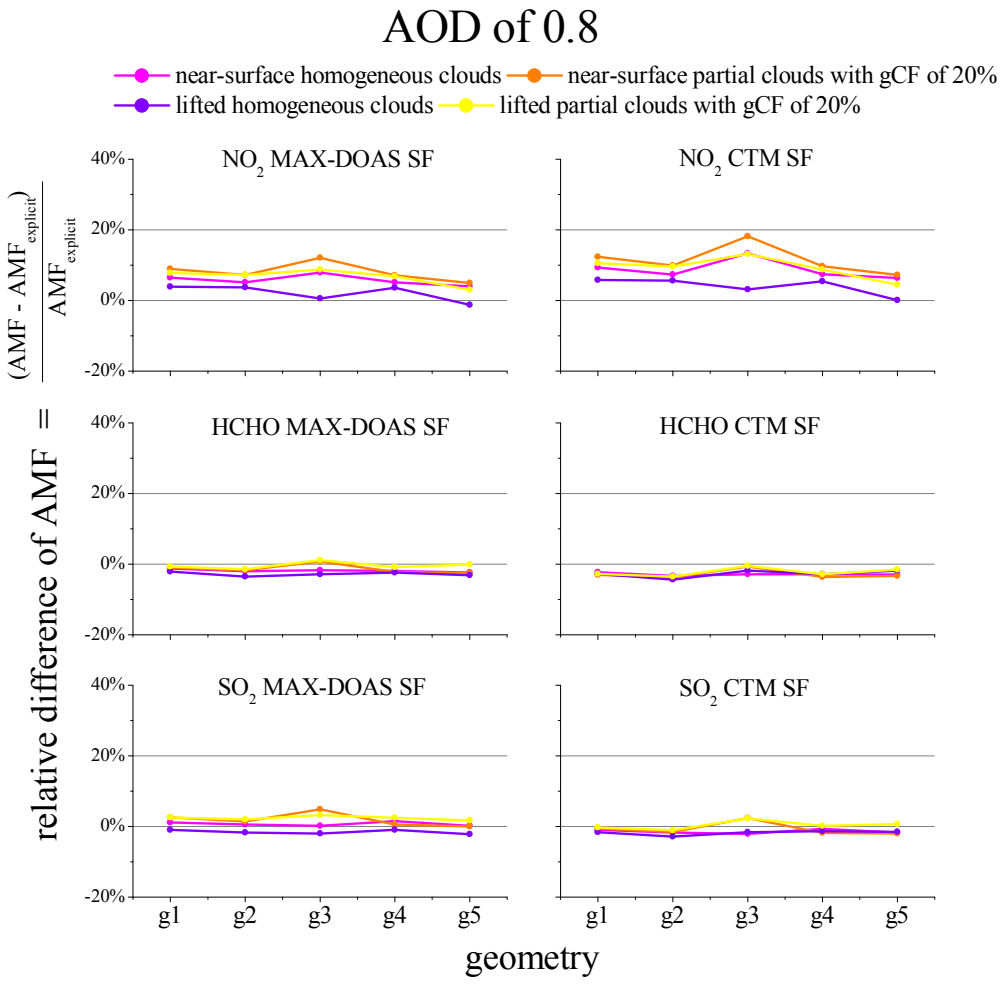

(b)

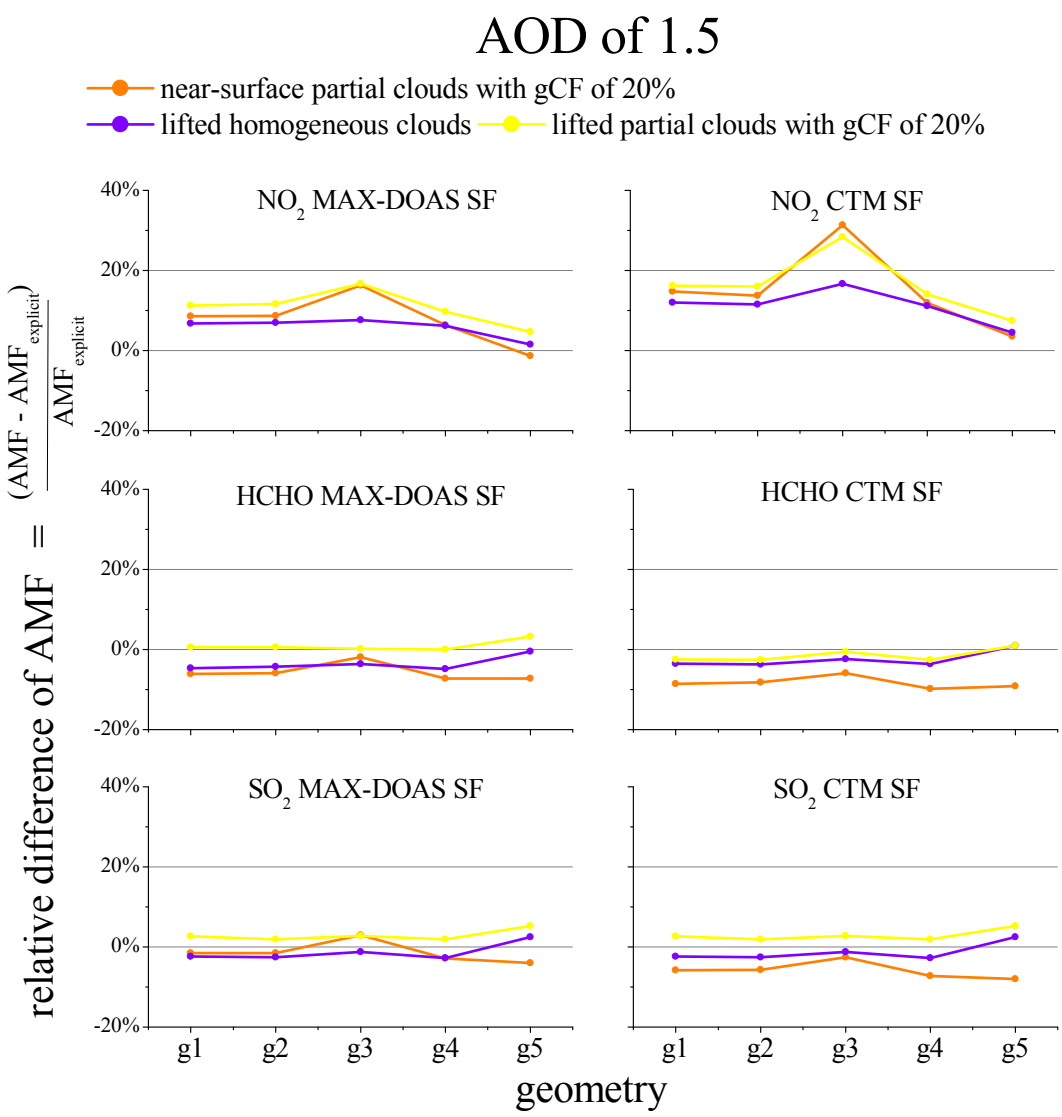

Figure S11: Relative differences of the three TG AMFs for the four cloud types and the corresponding aerosol profiles. The different labels at the x-axis indicate different observation geometries (see Table 2). The MAX-DOAS and CTM SFs are used for the calculations shown in the left and right columns. The aerosol profiles of AOD of 0.8 and 1.5 are used in subfigure (a) and (b), respectively.

4 Other figures

(a)

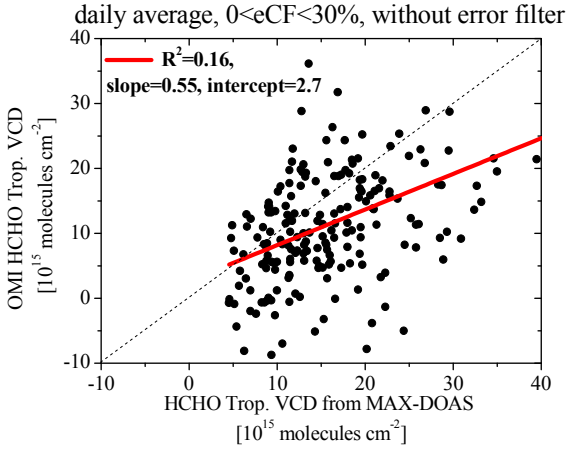

(b)

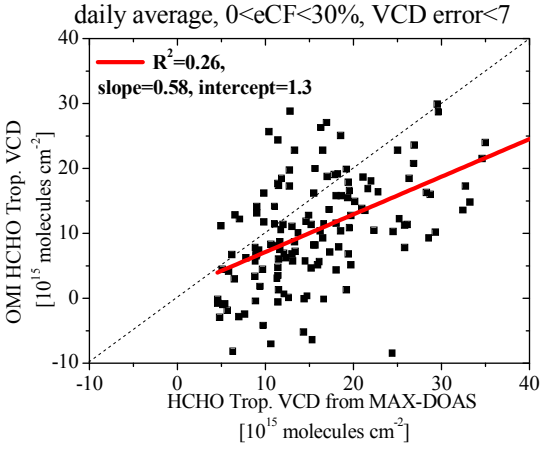

Figure S12: daily averaged HCHO tropospheric VCD derived from OMI observations are plotted against those derived from MAX-DOAS observations for eCF<30%. And linear regressions are also shown. The OMI data before and after the filter of VCD fit error < 7×10^{15} molecules cm^{-2} are plotted in subplot (a) and (b), respectively.

(a) OMI

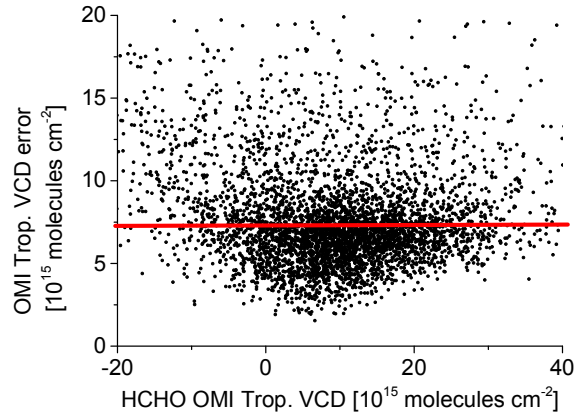

(b) GOME-2A

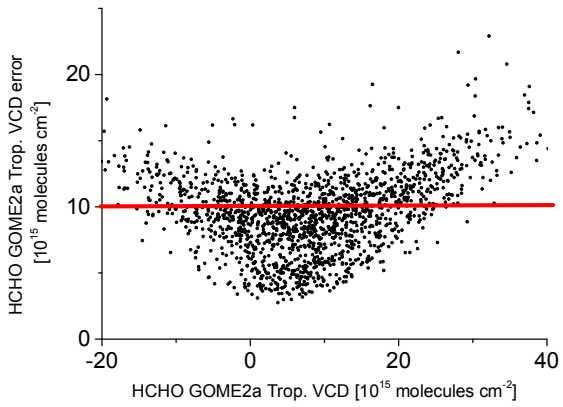

(c) GOME-2B

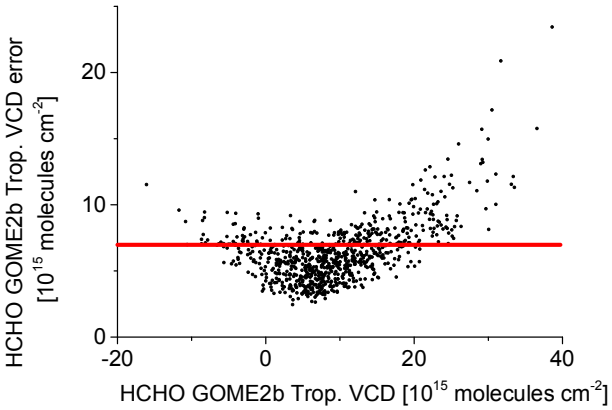

Figure S13: HCHO tropospheric VCDs for OMI pixels for eCF<30% are plotted against those derived from MAX-DOAS observations with the color map of eCF; the linear regression parameters are acquired for eCF<30% and for eCF<10%, respectively. (b) Scattered plots are same as in (a)

(a)

(b)

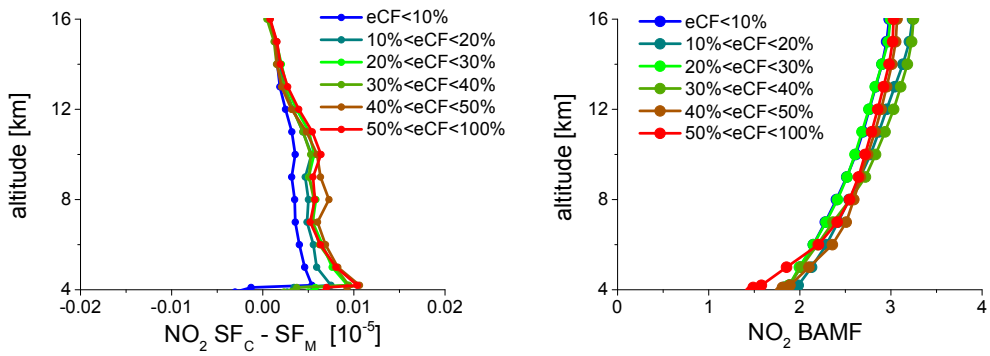

(c)

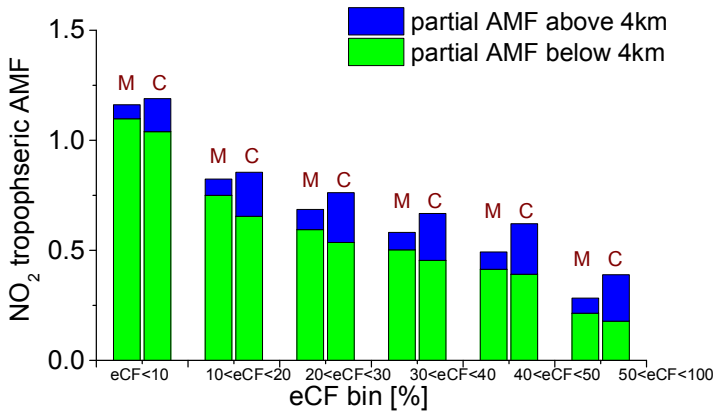

Figure S14: (a) Averaged difference between the NO_2 SF from CTM (SF_C) and from MAX-DOAS (SF_M) for different eCF bins in the altitude range of 4km to 16km. (b) Averaged NO_2 BAMF for satellite observation for different eCF bins in the altitude range of 4km to 16km. (c) NO_2 tropospheric AMFs calculated with averaged SF_M (marked by "M") and SF_C (marked by "C"), respectively; the partial AMFs below and above 4km are marked by green and blue columns, respectively.

(a) (b)

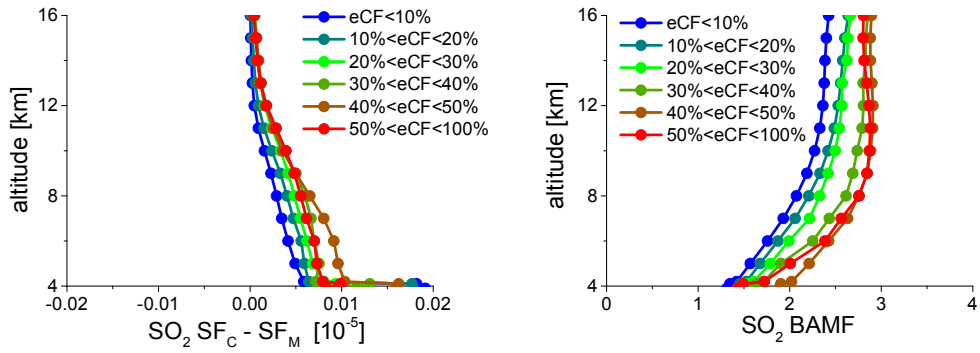

(c)

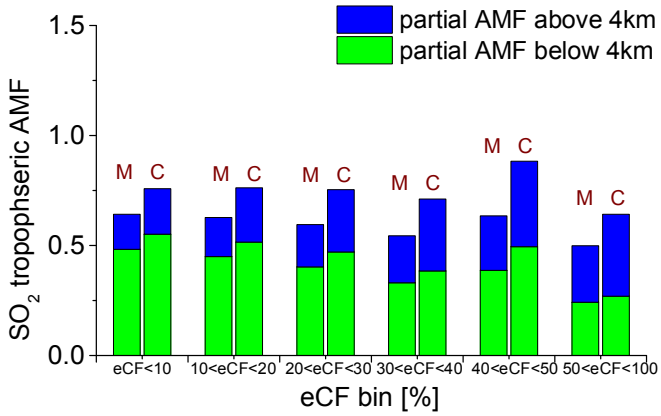

Figure S15: Same as Fig. S14, but for SO_2.

(a)

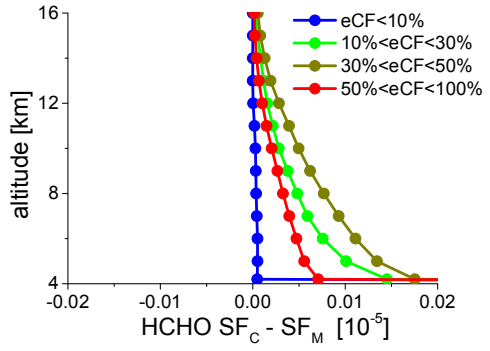

(b)

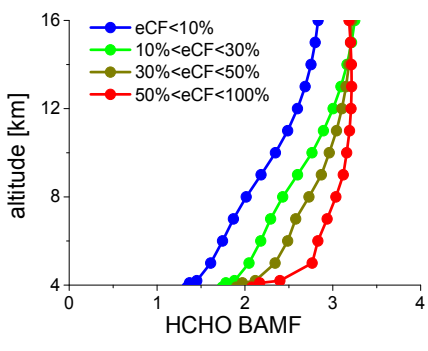

(c)

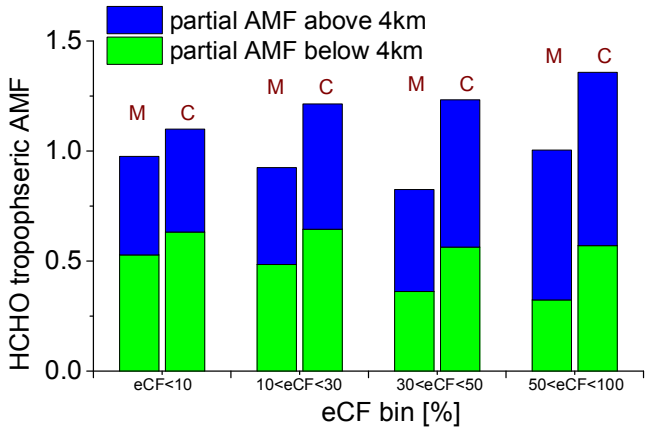

Figure S16: Same as Fig. S14, but for HCHO.

(a)

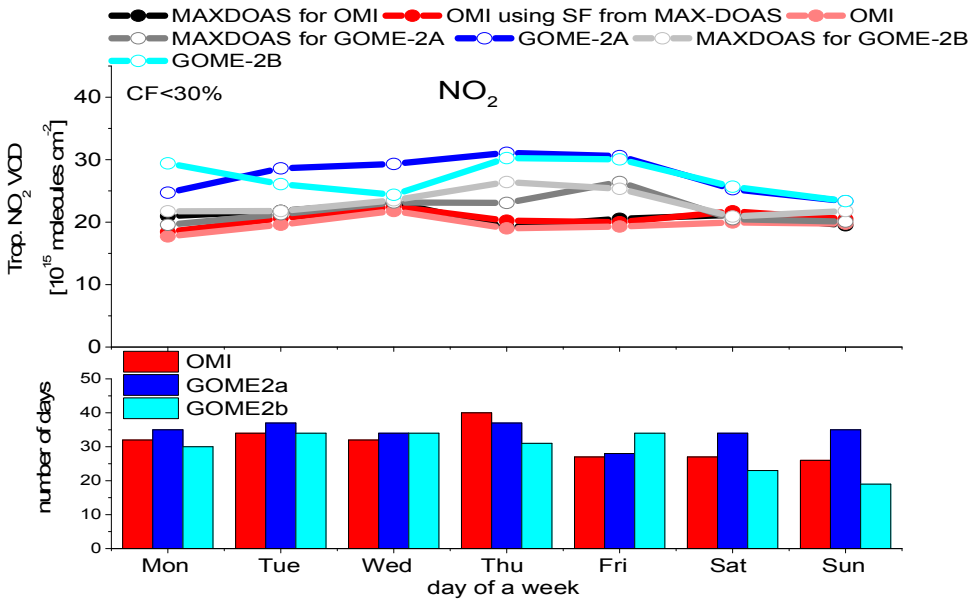

(b)

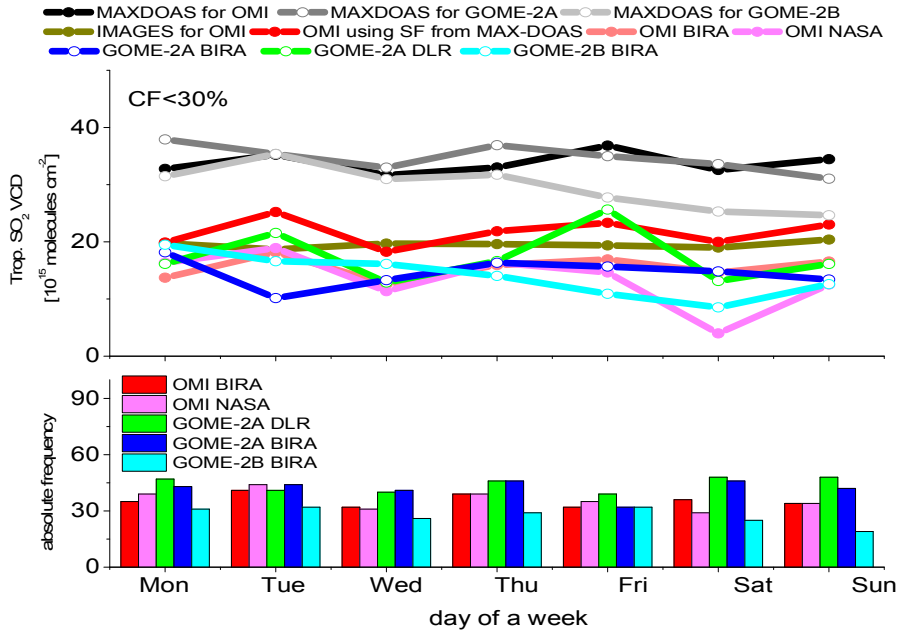

(c)

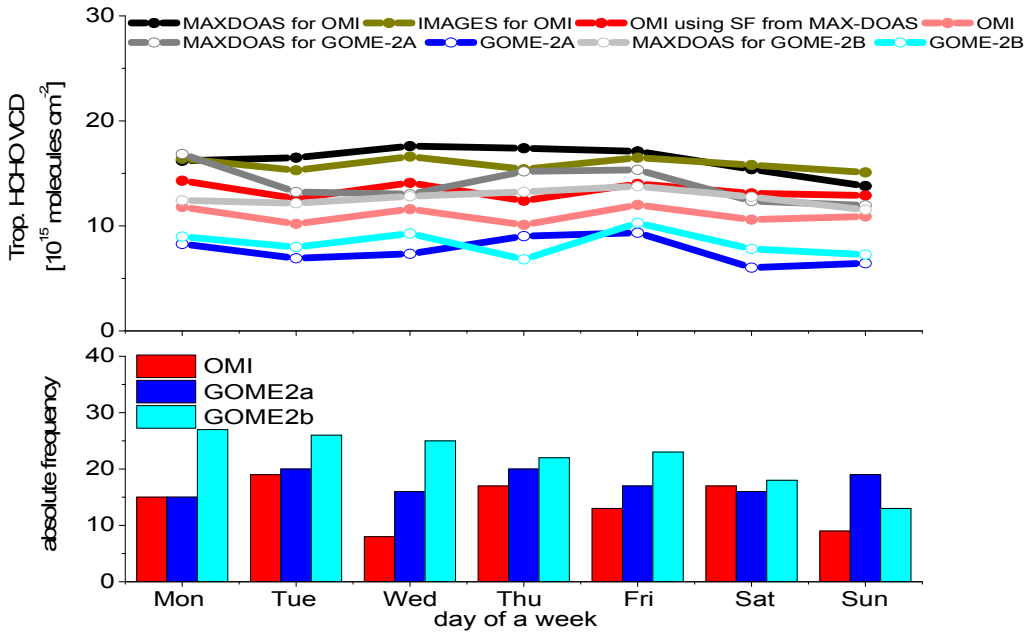

Figure S17: For eCF<30%, weekly cycles of VCDs of NO_2 (a), SO_2 (b) and HCHO (c) derived from different satellite instruments, corresponding coincident MAX-DOAS measurements. In all the subfigures the red and light red lines indicate the improved OMI tropospheric VCDs using the SFs from MAX-DOAS and the original VCDs from OMI products, respectively. The numbers of the available days in each two-month bin from different satellite products are shown in the bottom of each subfigure.

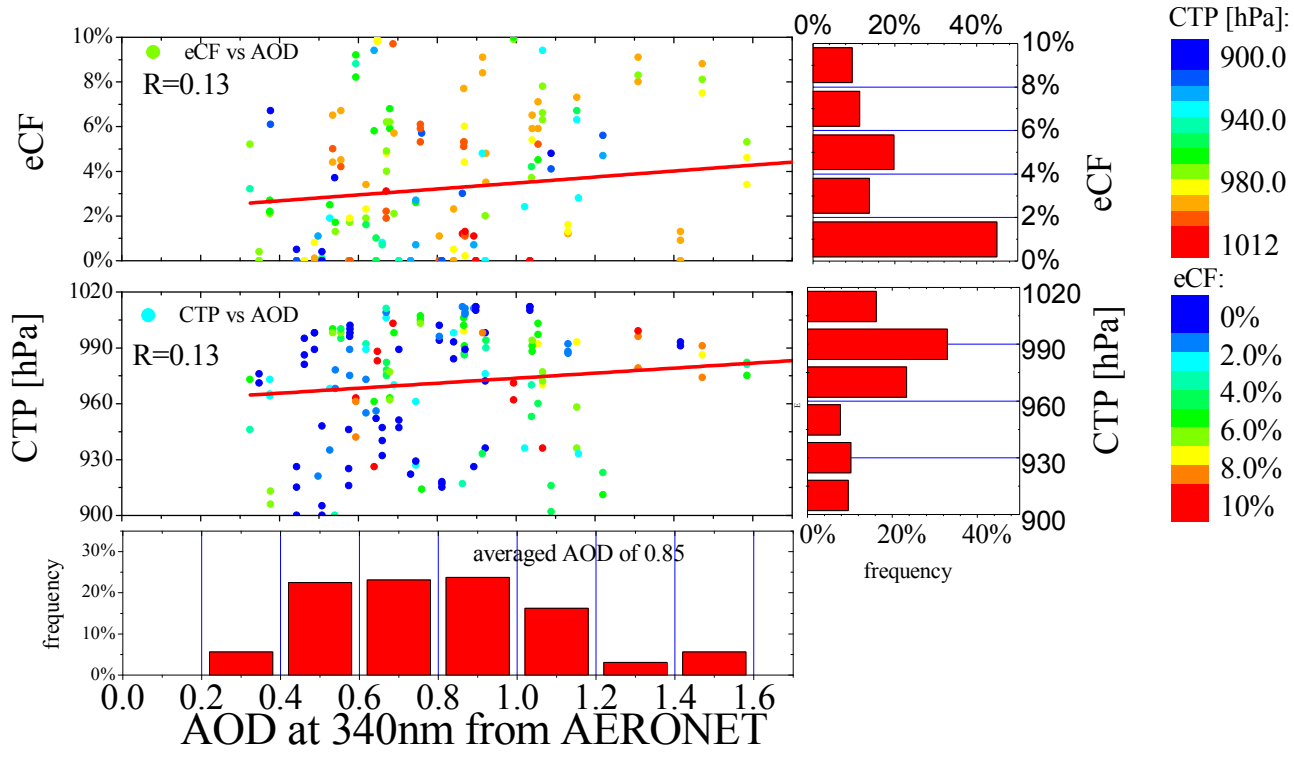

Figure S18: eCF and CTP from individual OMI observations are plotted against AOD around 360nm derived from AERONET Taihu station during the whole measurement in the condition of eCF<10% and CTP > 900hPa. The red bars on the right and bottom indicate the frequency of eCF, CTP, and AOD in different value intervals. The red lines are the linear regressions of the scatter plots. The correlation coefficients are shown in the plots. The color map in (a) and (b) indicate CTP and eCF, respectively.

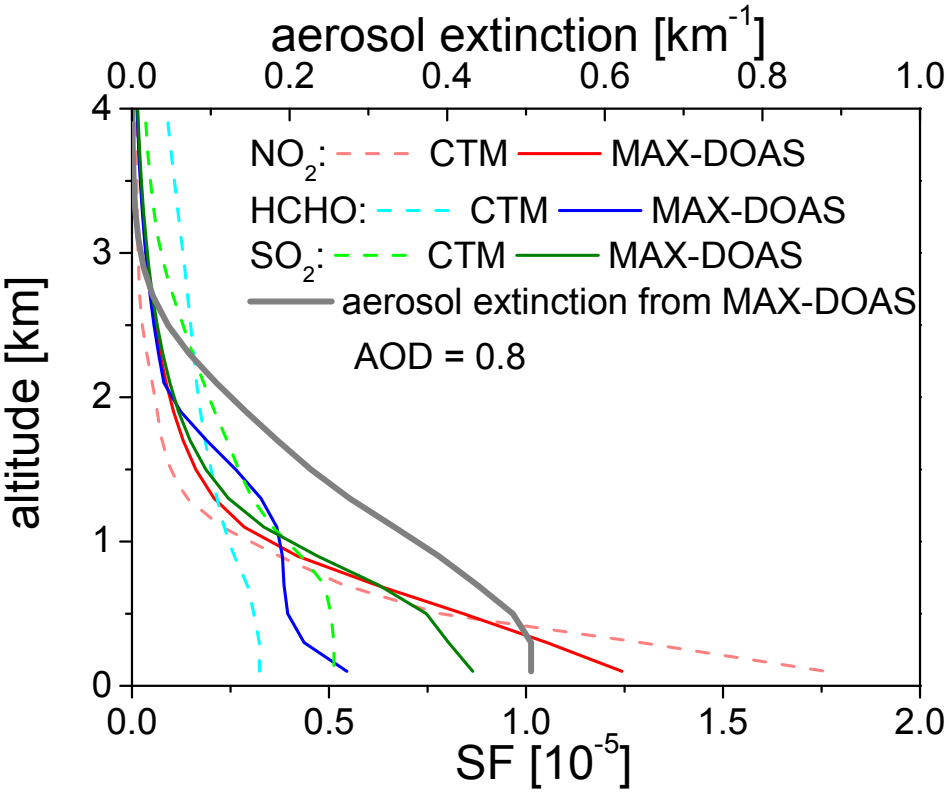

Figure S19: Averaged aerosol extinction profiles and SF of NO_2, SO_2 and HCHO derived from all MAX-DOAS measurements under cloud-free sky conditions. The dashed curves indicate the corresponding averaged SF derived from CTM simulations for NO_2 (TM4), SO_2 (IMAGES) and HCHO (IMAGES).